Research Article

Performance Evaluation of Forward Osmosis Membranes for Desalination Applications

Mohd Amirul Mukmin Abdullah [a,b]*, Nur Aisyah Shafie [c], Mazrul Nizam Abu Seman [b,c]* and Syamsul B. Abdullah [c]

[a] Forest Products Division, Forest Research Institute Malaysia, 52109, Kepong, Selangor, Malaysia

[b] Centre for Sustainability of Mineral and Resource Recovery Technology, Universiti Malaysia Pahang Al-Sultan Abdullah, Lebuh Persiaran Tun Khalil Yaakob, 26300 Kuantan Pahang, Malaysia

[c] Faculty of Chemical and Process Engineering Technology, Universiti Malaysia Pahang Al-Sultan Abdullah, Lebuh Persiaran Tun Khalil Yaakob, 26300 Kuantan, Pahang, Malaysia

*Author for correspondence; e-mail: amirulmukmin731@gmail.com, mazrul@umpsa.edu.my

ABSTRACT

Forward osmosis (FO) has become a technology with great potential for numerous applications, including water desalination. One of the critical factors in determining the FO performance is the selection of the appropriate membrane material that compatible with draw solution. In this study, commercial cellulose triacetate (CTA) and aquaporin-based membranes, as well as a fabricated PES/PVP membrane, were used, with 1-Butyl-3-methylimidazolium tetrafluoroborate ([Bmim][BF_4]) as the thermo-responsive ionic liquid (TRIL) draw solution. The bench scale of FO system was setup upon co-currently flow rate of 60.0 mL/ min at room temperature. The 7 % PVP with 15 % PES had the best performance, with the highest water flux (J_w) (4.93 LMH), lowest reverse solute diffusion (RSD) (0.43 gMH). The fabricated membrane demonstrated a significantly higher performance compared to the commercial aquaporin-based FO membrane, with an improvement of approximately 60%.

Keywords: forward osmosis, membrane, water process, desalination, ionic liquids

1. INTRODUCTION

Forward osmosis (FO) has gained popularity as a promising technology for desalination due to its low-pressure capability and energy-efficient operation, making it an attractive solution for seawater desalination. The process involves natural diffusion using osmotic pressure, whereby water molecules are drawn from a solution containing low solute concentration to a solution containing high solute concentration. The performance of the FO process is heavily dependent on the properties of the membrane used, including its selectivity, permeability, and stability [1]. As a result, considerable efforts have been made to develop and optimize FO membranes to enhance their performance. In order to be considered high-quality, FO membranes should exhibit several key characteristics. These include the ability to allow a high-water flux, while preventing the permeation of salts. Additionally, FO membranes should minimize concentration polarization, resist membrane fouling, and maintain their performance even when exposed to various chemicals [2–4].

The company HTI has introduced first-generation FO membranes, such as the nonwoven (HTI-NW)

and embedded support (HTI-ES) FO membranes, to the market. These membranes have an asymmetric structure, where the dense active layer is made of cellulose triacetate (CTA) and is cast with a polyester mesh embedded in it. To maintain its ability to reject contaminants and structural integrity while enhancing water permeability, the active layer thickness of the membrane is minimized [5].

On the other hand, HTI and OasysWater company were the pioneers in introducing the next generation of FO membranes, which are known as thin film composite (TFC) membranes. These membranes were designed to overcome the limitations of CTA membranes. TFC membranes have comparable rejection rates to CTA membranes, but they are capable of significantly improving water flux rates to approximately 30-40 LMH, compared to the 10 LMH achieved by CTA membranes [6]. Moreover, TFC membranes provide more flexibility in structural design since the selective layer and substrate layer can be independently adjusted to meet specific requirements. The typical procedure for creating TFC membranes, according to Goh et al., (2019), involves using phase inversion casting to obtain a microporous substrate, followed by interfacial polymerization (IP) between amine and chloride monomers to create a polyamide (PA) selective layer. Reactive monomers, such as trimesoyl chloride (TMC) and m-phenylenediamine (MPD) are commonly used to form the PA layer in FO membranes [7]. Recently, Aquaporin A/S has developed a novel arrangement of hollow fiber membranes that provides a greater packing density compared to the conventional spiral wound configuration [8]. These membranes utilize aquaporin proteins as pore-forming agents in the thin film layer, facilitating water diffusion through passive facilitated transport. This unique design allows the protein to maintain its geometrical structure during operation, resulting in selective water transport that is 5 to 1000 times higher than that of conventional membranes [9]. As a result, Aquaporin-assisted membranes offer the potential for significantly greater permeability compared to traditional membranes [10]. The market has seen a surge in the number of global FO membrane suppliers, providing more competitive options [11]. Details of the currently available commercial FO membranes can be found in Table 1.

Table 1. Summary of the commercial FO membranes.

Supplier	Materials/Commercial Name	Configurations
HTI	CTA-NW	SW
HTI	CTA-ES	SW
HTI	TFC	SW
Aquaporin A/S	Aquaporin	SW, HF
OasysWater	TFC	SW
Porifera	PFO element	SW
Toray	FO membrane	SW
Fluid technology solution	CTA	SW
Modern water	-	SW
Toyobo	-	HF
Trevi System	-	SW

*SW – spiral wound, HF – hallow fibre

Polyvinylpyrrolidone (PVP) is widely used as an additive in various membrane frameworks, including forward osmosis (FO) membranes. Its popularity stems from its non-toxicity and compatibility with water and a range of organic solvents. Recent studies have highlighted the promising role of PVP as a polymer additive, offering multiple benefits such as enhancing rejection rates, acting as a swelling agent, improving pore characteristics, preventing fouling, suppressing macropores, and enhancing hydrophilicity [12]–[15]. The PVP are commonly added to the casting solution of PES to create filtration membranes. Polyether sulfone (PES) membrane are commonly used in biomedical areas and water desalination [16]. As reported by Alvi et al., (2019), PES is the most hydrophilic sulfone group polymer due to its high number of moieties in the polymer repeating unit of the sulfone group [17]. This, combined with its high mechanical strength, chemical resistance, and stability in a pH range of 2 to 13, make it an ideal choice for a membrane material [18]. Furthermore, PES is soluble in aprotic polar solvents such as N-Methyl-2-pyrrolidone (NMP), dimethylformamide (DMF), and other similar solvents [18 - 19].

One of the main challenges in creating FO membranes is achieving a balance between high water permeability and efficient salt rejection or RSD. Selecting an appropriate FO membrane and draw solute is crucial in achieving successful desalination. Thermo-responsive ionic liquids (TRILs) are being studied as a potential draw solute for FO processes. While most ionic liquids are classified as either hydrophilic or hydrophobic based on their solubility in water at room temperature, the solubility of some ILs can vary depending on temperature, making their properties ambiguous [21].

According to Akther et al., (2015), the use of thermo-responsive draw solutions in FO hybrid systems leads to reduced energy consumption when desalinating saline waters, potentially making it a more economically viable option than other de-salination technologies [22]. Many researchers have conducted extensive studies on utilizing TRIL such as tetrabutylphosphonium trifluoroacetate $[P_{4444}^+]$ [CFOO], tetrabutylphosphonium p-toluenesulfonate $[P_{4444}^+][TsO]$, poly(1-butyl-3-vinylimidazolium) Bis(trifluoromethylsulfonyl)imide $[Ntf_2][vmim]$, tetrabutylammonium 2,4,6-trimethylbenzene sulfonate $[N_{4444}^+][TMBS]$, Tetrabutylammonium 2,4-dimethylbenzene sulfonate $[N_{4444}^+][DMBS]$, Betaine Bis(trifluoromethylsulfonyl)imide [Hbet] $[Ntf_2]$ and many more in desalination processes, paving the way for their potential application in addressing water scarcity and advancing sustainable water treatment technologies [23]–[27].

Figure 1 demonstrated the potential for utilizing TRILs as a draw solution in the development of a technique for extracting low-concentration water from saline water. The performance of Aquaporin and cellulose triacetate (CTA) FO commercial membranes were compared with a PES/PVP fabricated membrane containing varying concentrations of PVP. The draw solution chosen was one of the best TRILs identified in a previous study, namely 1-butyl-3-methylimidazolium tetrafluoroborate $([Bmim][BF_4])$ [28]. While previous studies have investigated the performance of commercial FO membranes and draw solutions, this study focuses on the fabrication and evaluation of a novel PES/PVP membrane and the use of thermo-responsive ionic liquids (TRILs) as draw solutions, providing new insights into membrane selection for FO desalination applications. The membrane's stability was assessed through the measurement of water flux and FESEM characterization.

2. MATERIALS AND METHODS
2.1 Material and Equipment

Polyethersulfone (PES, Petronas BASF Malaysia), polyvinylpyrrolidone (PVP, Molecular weight~40,000g/mol, Sigma Aldrich), and 1-methyl-2-pyrrolidinone (NMP, 99%, Sigma Aldrich) were used to fabricate PES substrate. For active layer formation, M-Phenylenediamine (MPD, flakes, 99%,
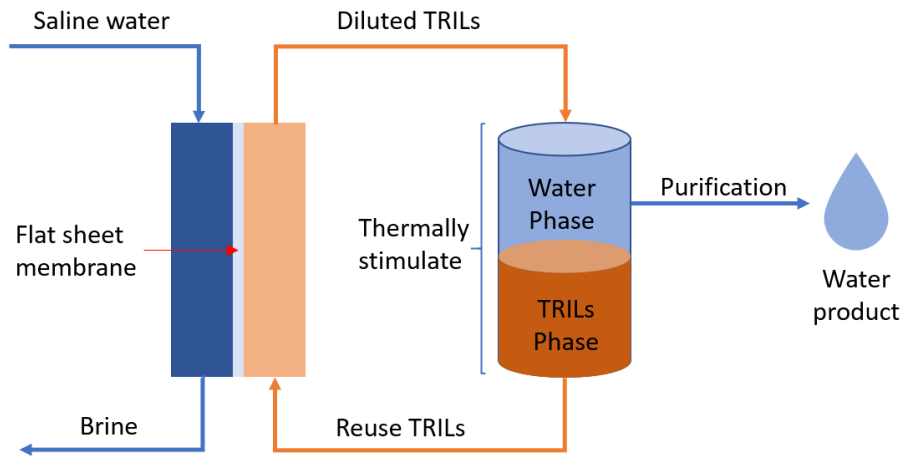
Figure 1. FO process schematic diagram.

Sigma Aldrich) in deionized (DI) water and 1,3,5-Benzenetricarbonyl chloride (TMC, Sigma Aldrich) in hexane (Emsure®, Supelco) were utilized. Flat sheet FO membrane was purchased from HTI Technology (USA) and Aquaporin Inside (Denmark). 1-butyl-3-methylimidazolium tetrafluoroborate ([Bmim][BF$_4$]), Sigma Aldrich with purity 98% and sodium chloride were used as draw solution.

2.2 Support/substrate Layer Fabrication
2.2.1 Dope solution preparation
The dope solution which consisted of polyethersulfone (PES) polymer, polyvinylpyrrolidone (PVP) and N-methyl-2-pyrrolidone (NMP) will be mixed to produce the homogenous dope solution based on previous study [29]. The mixture then will be stirred vigorously at 300 rpm at room temperature until the honey-like texture solution obtained. Prior to the casting process, the dope solution will be left for a period of time to remove air bubbles that have formed due to stirring.

2.2.2 Casting of porous support layer
The fabrication of support layer will be done using semi-automated casting machine. The casting knife thickness will be adjusted accurately to form neat and uniform membrane

layer. The porous support layer will be produced by pouring the appropriate amount of dope solution onto the glass plate and let the casting knife to scatter the solution evenly. Gently and speedily, the dope film on the glass plate will be soaked into the coagulation bath to allow the phase inversion process. After 1-2 minutes, the white film/membrane or membrane substrate layer will automatically peel off from the glass plate. The membrane layer will be stored and soaked in deionized water overnight to remove the excess solvent.

2.3 Active Layer Formation
For the formation of polyamide layer, two immiscible solutions; MPD and TMC solution are used. The 2 wt% of MPD solution will be prepared by dissolving 2 g of MPD palette in 100ml of distilled water. Meanwhile, 0.15 g of TMC will be dissolved in 100 mL of hexane to form TMC solution with 0.15 wt% of concentration. The porous support membrane produced will be cut into square shaped and clamped horizontally using acrylic frame before pouring MPD solution on the top of membrane surface for 10 minutes. After removing the excess MPD from the surface, TMC will be poured onto the MPD coated membrane and left out for 2 minutes to complete the interfacial

polymerization process. The thin film composite (TFC) FO membrane produced will be dried in an oven for 5 minutes to evaporate the excess hexane and stored in a container containing deionized water until further use.

2.4 Membrane Morphology Characterization

The surface and internal structures of both the fabricated and commercial membranes were analyzed using a field emission scanning electron microscope (FESEM) JSM-7800F model from JEOL Ltd. The samples were coated with gold before imaging with FESEM. The FESEM images were captured at different magnifications with range 100 to 30 000 times under a vacuum condition of 5 kV for better resolution.

2.5 Forward Osmosis Experiment Setup

A laboratory-scale circulating arrangement was employed to carry out FO experiments by using commercial Aquaporin (AQP), HTI cellulose triacetate (CTA) and fabricated flat sheet membrane. Two types of feed solution of 0.04 M of NaCl (brackish water) and 0.6 M of NaCl (sea water) and two type of draw solution of NaCl and selected TRILs with concentration 0.04 – 0.20 M (brackish water) and 0.6 – 3.0 M (sea water) were tested in the FO experiment. 100 mL of feed solution and draw solution were used to carry out the FO process at room temperature. A peristaltic pump was utilized to circulate the feed and draw solutions in a loop on either side of the membrane cell, with a co-current flow rate of 60.0 mL/min. [30]. The membrane was vertically placed inside the membrane cell, creating two compartments: one for the feed solution and the other for the draw solution. The orientation of the membrane was determined by the filtration mode being used. In FO mode, the active layer of the membrane faced the feed solution channel, while in PRO mode, it faced the draw solution. The initial conductivity of the feed solution was measured.

The experiment was conducted using the "One Factor at a Time" (OFAT) method. Initially, the performance of the commercial membrane was evaluated, followed by an assessment of membrane orientation. Once the best commercial membrane and orientation were identified, they were compared with the performance of the fabricated membrane.

2.6 Determination of Water Flux and Reverse Salt Flux

The water flux, J_w (LMH) was determined by monitored the weight of the draw solution using a computer-linked balance. The data was automatically exported at 5-minute intervals until the process was complete. The water flux was calculated using (Eq. 1) [31]:

$$J_w = \frac{\Delta V}{A_m . \Delta t} \tag{1}$$

where ΔV(L) is the volume change of the feed solution over a time Δt(h) A_m(m^2) is the effective membrane surface area.

The reverse solute diffusion, RSD (gMH) was calculated from the concentration and volume change of the feed solution using Eq. (2) [32]:

$$RSD = \frac{\Delta(CV)}{A_m . \Delta t} \tag{2}$$

where C (mg/L) and V (L) are the total dissolved solid concentration in the feed and the feed volume, before and after a predetermined operation time Δt (h). The final conductivity value of the feed solution was taken and recorded. C (mg/L) could be accurately detected by a calibrated conductivity meter (Mettler Teledo, Model FE38).

3. RESULT AND DISCUSSION
3.1 Membrane Morphology Characterization using FESEM

FESEM was utilized to examine the morphologies and surface characteristics of the membranes. Figure 2 and 3 illustrate the FESEM

images of the top and bottom Aquaporin (AQP), CTA, and PES/PVP membranes. The CTA membrane's active surface was smooth (figure 2(a)), whereas the AQP membrane exhibited rough ridge-and-valley features (figure 2(b)). The PVP membranes (11% and 7%) had a typical structure resembling the AQP membrane (figure 2(c) and (d), respectively), with surface roughness increasing as the percentage of PVP decreased. The excessive of PVP will cause the dope solution's viscosity to rise. This increased viscosity hinders the exit of PVP from the polymer-rich phase, leading to a membrane structure with reduced pore formation and roughness [33]. Meanwhile, the roughness of the AQP membrane surface indicates typical polyamide surface features [34].

According to Chun et al., (2018), this roughness is attributed to the AQP-containing vesicles, which have diameters ranging from 100 to 200 nm [35]. These vesicles maintain their original properties and integrity due to the incorporation of AQP, enabling higher permeate water flux [36].

The support substrate of the FO membrane is an essential component that affects the membrane's stability, selectivity, and performance. Figures 3(a)-(d) provide a comparison of the support substrates for the CTA and AQP FO membranes. The AQP membrane's nonwoven support appeared denser (Figure 3(b)) than that of CTA, which had a woven mesh support layer (Figure 3(a)). The nonwoven support of AQP is known to provide enhanced structural stability
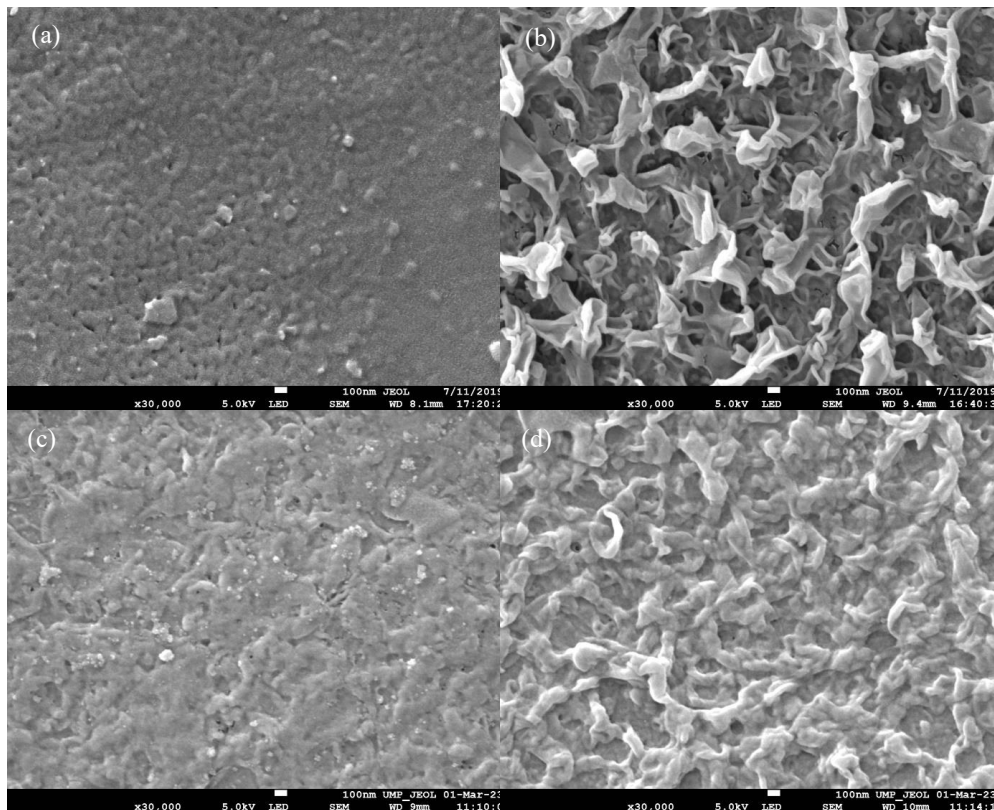

Figure 2. Top surface FESEM image at magnification 30,000x of CTA (a), aquaporin (b), PVP 11% (c) and PVP 7% (d).
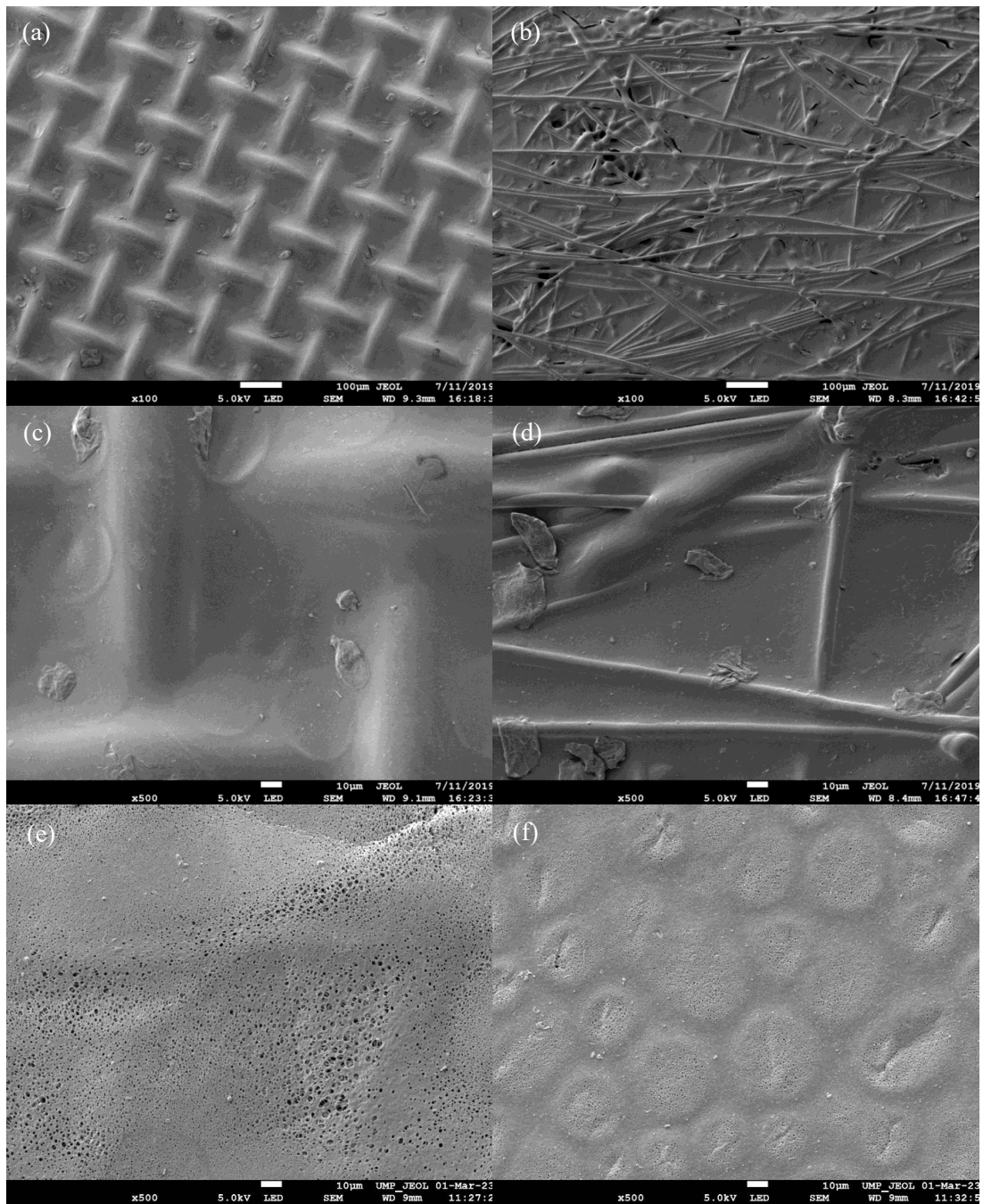
Figure 3. Bottom surface FESEM image at magnification 100x of CTA (a), aquaporin (b) and 500x and CTA (c), aquaporin (d), 11% PVP (e) and 7% PVP (f).

and improved mechanical properties, leading to higher durability and longer operational lifespan. On the other hand, the woven mesh support of CTA provides higher porosity, which promotes better water permeability but also lower tortuosity, which can decrease the membrane's selectivity [16].

The woven mesh support layer present in the CTA membrane led to a highly non-uniform membrane thickness, with regions away from the mesh fibers being thinner than those near the fibers. This non-uniformity had a significant impact on the internal concentration polarization (ICP) phenomenon that occurs during FO processes. ICP causes the concentration of the solutes in the boundary layer adjacent to the membrane to increase, leading to a reduction in water flux. The presence of the woven mesh support layer in CTA contributed to a more significant ICP compared to AQP, which had a more uniform membrane thickness and higher water flux [28 - 29]. Overall, the differences in support substrate characteristics between AQP and CTA membranes can significantly affect FO process performance, emphasizing the importance of choosing an appropriate support substrate for FO membrane fabrication.

Another aspect of membrane fabrication that affects the membrane structure and properties is the concentration of the polymer used in the casting solution. Figures 3(e) and (f) show the difference in pore distribution between membranes produced with 7% and 11% PVP concentration, although their sponge-like and porous web structure appears identical. Numerous studies have demonstrated that TFC membranes with an ideal support layer characterized by a thin sponge-like structure offer significant advantages in terms of their ability to withstand high pressures and achieve high performance [39], [40]. At the same magnification, the membrane with 7% PVP displayed a more uniform pore size and distribution compared to the 11% PVP membrane. The larger amount of PVP in the 11% PVP membrane slowed down the precipitation process, resulting in slower demixing, particularly in the bottom layer of the membrane

(closest to the glass slide) [13]. These differences in pore distribution can impact the membrane's permeability and selectivity, highlighting the importance of best condition in casting solution composition in membrane fabrication.

3.2 Forward Osmosis Performance
3.2.1 Effect of membrane type

This study compared two types of commercially available FO membranes: one is composed of cellulose triacetate (CTA) with a polyester mesh embedded for mechanical support, which has been extensively used in various FO processes and research. The second type is a relatively new membrane composed of a thin-film composite (TFC) membrane, where aquaporin proteins are embedded in a polyamide layer to stabilize vesicles. It is supported by a porous polysulfone layer [41]. In the experiment, the draw solution was composed of 0.08 M NaCl and [Bmim][BF$_4$], while the feed solution contained 0.04 M NaCl. The water flux results were presented in Figure 4, and it was observed that the AQP membrane exhibited better performance in terms of water flux compared to the CTA membrane. Specifically, the recorded water flux with the AQP membrane was around 0.98 LMH, which was 25% higher than that of the CTA membrane. This finding is consistent with a previous study conducted by Xia et al., (2017), which also demonstrated the superior water flux performance of the AQP membrane. As a result, the Aquaporin membrane was selected for the remainder of the study due to its better water flux performance [42].

Furthermore, Figure 4 shows that [Bmim][BF$_4$] generates higher water flux compared to NaCl. This is attributed to the higher draw ability of [Bmim][BF$_4$] due to its higher degree of ionic liquid association in water, as indicated by the predicted Van't Hoff factor. The predicted Van't Hoff factor (i) for [Bmim][BF$_4$] reported in previous study is 2.19 by using group contribution method (GCM) [43]. In ideal conditions, i value would be 2 for completely dissociated charged
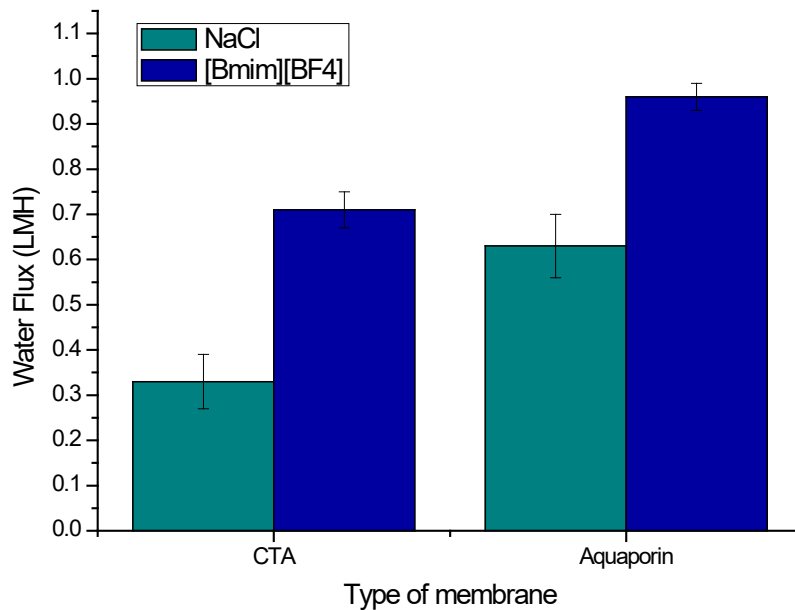
Figure 4. Comparison of water flux at different type of membrane.

species in water, but in real systems, ion pairing can occur, resulting in lower or higher i values. For instance, the experimental value for NaCl is $i = 1.89$. [44].

3.2.2 Effect of membrane orientation

To evaluate the performance of the Aquaporin membrane, two filtration modes were compared: FO mode and PRO mode. In FO mode, the active selective layer faced the feed solution, while in PRO mode, it faced the draw solution. The experimental setup used 0.08 M of [Bmim][BF$_4$] and NaCl as the draw solute and 0.04 M of NaCl as the feed solution, with the Aquaporin membrane as the filtration membrane.

The water flux values for both [Bmim][BF$_4$] and NaCl were measured for PRO and FO modes, and the results showed that the water flux values for [Bmim][BF$_4$] were 1.11 and 0.93 LMH for PRO and FO modes, respectively, while those for NaCl were 0.89 and 0.76 LMH for PRO and FO modes, respectively, as illustrated in Figure 5. Water flux values for both [Bmim][BF$_4$] and NaCl

were determined for PRO and FO modes, with [Bmim][BF$_4$] showing higher water flux values in both modes. The water flux in PRO mode was approximately 15% higher than that in FO mode, which can be attributed to the presence of internal concentration polarization (ICP) in the porous layer of the membrane that affects osmotically driven membrane processes. Previous studies have shown that ICP can significantly reduce water flux in FO, with reductions of over 40% reported [34 - 35].

The phenomenon of internal concentration polarization (ICP) occurs in osmotically driven membrane processes due to the asymmetrical structure of the FO membrane. Dilutive ICP occurs when the porous layer faces the draw solution in FO mode, and water permeates through the membrane to dilute the draw solution. Concentrative ICP, on the other hand, occurs when the porous layer faces the feed solution in PRO mode, and the solute from the feed cannot penetrate the active layer, leading to a concentrative polarization layer within the pore of the support
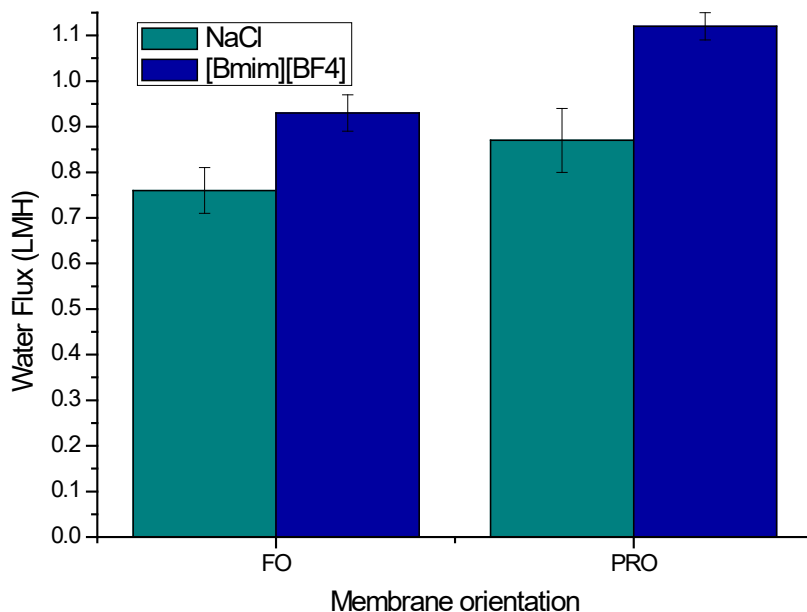
Figure 5. Comparison of water flux at different type of membrane orientation.

layer. Zhao et al., (2011) have reported that the feed solution and the degree of concentration are the key factors affecting the efficiency of the two modes. They also concluded that water flux is higher in PRO than in FO mode. Therefore, in this study, the PRO mode was chosen to achieve high water flux [47].

3.2.3 Effect of feed and draw solution concentration

Once the best membrane and orientation were identified based on their performance, the impact of feed and draw solution concentrations on water flux and reverse salt flux was investigated. Initially, the performance was tested using simulated brackish water with a concentration of 0.04 M NaCl, followed by testing with seawater with a concentration of 0.6 M NaCl. Various concentrations of draw solution, ranging from the same concentration as the feed solution up to five times higher, were used to obtain water flux and reverse so RSD measurements for [Bmim][BF$_4$]. According to the data presented in Figure 6, the

7% PVP membrane with 0.2 M of [Bmim][BF$_4$] draw solution achieved the highest water flux of 4.19 LMH, followed by AQP at 3.36 LMH, and the 11% PVP membrane at 2.56 LMH, using the same draw solution concentration. However, for the 11% PVP membrane with draw solution concentrations below 0.12 M, the RSD exceeded the water flux. Similarly, for the 7% PVP and AQP membranes with 0.04 M draw concentration, the reverse salt flux was also greater than the water flux. On the other hand, Figure 7 (seawater) revealed that the 5% PVP membrane achieved the highest water flux of 4.93 LMH at 3.0 M draw concentration, followed by AQP at 2.89 LMH, and the 11% PVP membrane at 2.67 LMH. However, the AQP membrane exhibited the highest RSD of 0.76 gMH, followed by the 7% PVP membrane at 0.69 gMH and the 11% PVP membrane at 0.45 gMH, at a draw concentration of 0.6 M [Bmim][BF$_4$].

The experimental results indicated that an increase in draw solution concentration led to a corresponding increase in water flux and a decrease in RSD in all cases. This can be attributed to
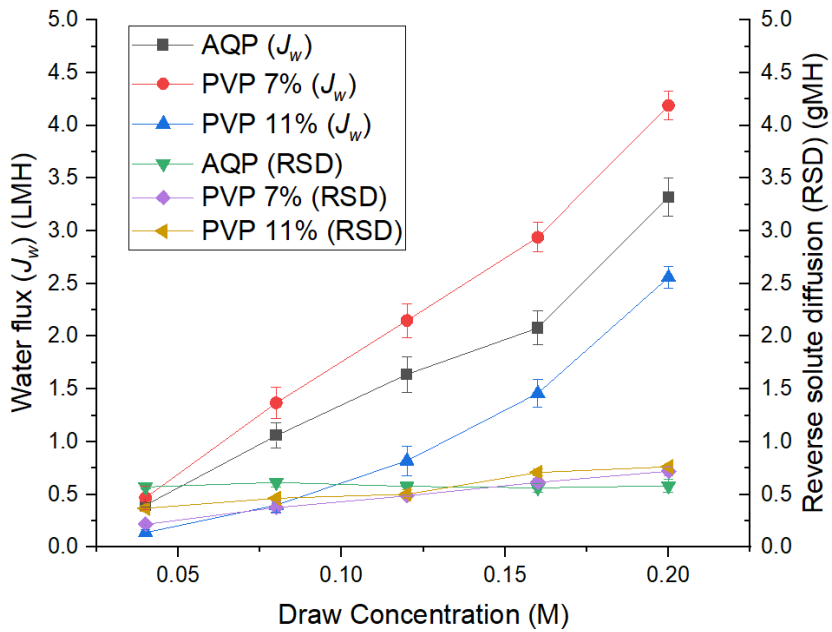
Figure 6. Water flux and RSD for brackish water as feed solution.
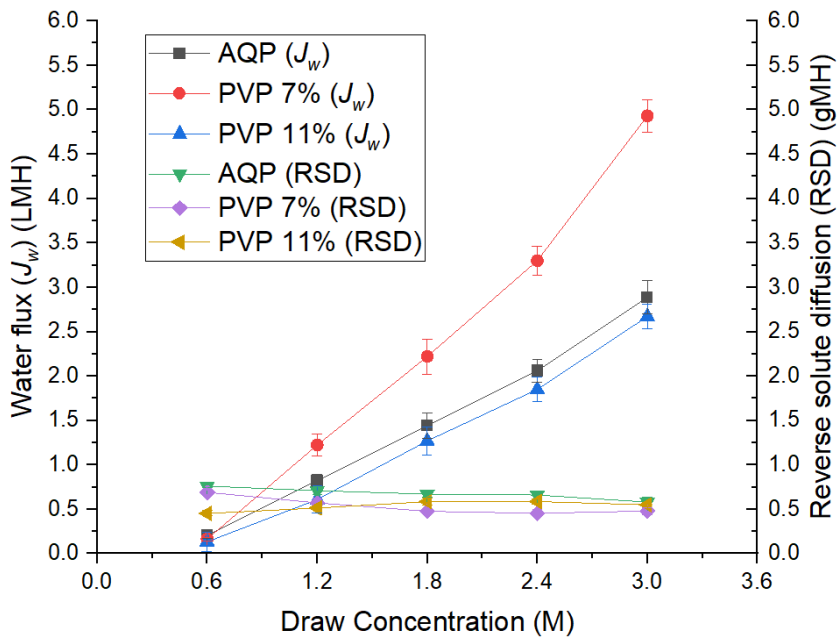

Figure 7. Water flux and RSD for seawater and as feed solution.

the higher osmotic pressure difference between the feed and draw solutions at higher draw concentrations, resulting in a reduction in salt retention and an increase in salt deposition on the membrane surface. This phenomenon resulted in a decrease in RSD from the draw to the feed solution. Similar observations were reported by previous studies such as Sivertsen et al., (2018) and Giagnorio et al., (2019) where a lower draw solution concentration produced a lower osmotic driving force, resulting in slower salt deposition on the membrane surface [37 - 38].

The permeability characteristics of a membrane are significantly influenced by the morphology of its top and bottom layers, including surface roughness and pore distribution. The membrane composed of 7% PVP and 15% PES was observed to have the highest water flux in this study. The reason behind this could be attributed to the morphology of the membrane, where the top layer was denser and rougher, while the bottom layer had a more porous structure. The rough and dense top layer provided a larger surface area for water molecules to permeate through, while the sponge-like bottom layer created more pathways for water to flow. This combination of a rough and dense top layer with a sponge-like bottom layer resulted in a membrane with the optimal pore distribution for water permeation.

4. CONCLUSIONS

In conclusion, two types of membrane had successfully fabricated in this study with different concentration of 7 % and 11 % PVP with 15% PES. The 7% PVP membrane achieved highest water flux which is 4.93 LMH with 0.48 gMH RSD using 3.0 M of $[Bmim][BF_4]$ as draw solution and artificial sea water 0.6 M of NaCl as feed solution. This fabricated membrane exhibited the highest water flux, which could be attributed to its unique morphology with a rough and dense top layer and a sponge-like bottom layer. It was also observed that increasing the draw solution concentration led to an increase in water flux and a decrease

in RSD, due to the higher osmotic pressure difference between the feed and draw solutions. However, excessive draw solution concentrations can lead to high reverse salt flux, which should be considered when optimizing the performance of FO desalination membranes.

Through this study, some recommendations are suggested to improve the overall FO process in terms of ILs selection. It is proposed that designing ILs as draw solutes or using FO membranes with high selectivity or low affinity towards specific ILs could enhance the efficiency of the FO process. Despite the lower membrane fouling tendency in FO compared to RO, further research should explore the potential corrosiveness of cellulose-based membranes when exposed to certain IL species, as previous studies indicate a possibility of cellulose dissolution [50], [51]. Overall, the findings of this study can contribute to the development of more efficient and effective membranes for FO desalination applications.

REFERENCES

[1] Sigh S.K., Sharma C. and Maiti A., *J. Environ. Chem. Eng.*, 2021; **9(4)**: 105473. DOI 10.1016/j.jece.2021.105473.

[2] Chung T., Zhang S., Yu K., Su J. and Ming M., *Desalination*, 2012; **287**: 78–81. DOI 10.1016/j.desal.2010.12.019.

[3] Xu W. and Ge Q., *J. Membrane Sci.*, 2018; **555**: 507–516. DOI 10.1016/j.memsci.2018.03.054.

[4] Hadadpour S., Tavakol I., Shabani Z., Mohammadi T., Tofighy M.A., and Sahebi S., *J. Environ. Chem. Eng.*, 2021; **9(1)**: 104880. DOI 10.1016/j.jece.2020.104880.

[5] Li J., Ni Z., Zhou Z., Hu Y., Xu X. and Cheng L., *J. Membrane Sci.*, 2018; **552**: 213–221. DOI 10.1016/j.memsci.2018.02.006.

[6] Valladares Linares R., Li Z., Sarp S., Bucs S. S., Amy G. and Vrouwenvelder J.S., *Water Resour.*, 2014; **66(4)**: 122–139. DOI 10.1016/j.watres.2014.08.021.

[7] Goh P.S., Ismail A.F., Ng B.C., and Abdullah M.S., *Water*, 2019; **11(10)**: 2043. DOI 10.3390/w11102043.

[8] Alshwairekh A.M., Alghafis A.A., Alwatban A.M., Alqsair U.F., and Oztekin A., *Desalination*, 2019; **460**: 41–55. DOI 10.1016/j.desal.2019.03.003.

[9] Giwa A., Hasan S.W., Yousuf A., Chakraborty S., Johnson D.J., and Hilal N., *Desalination*, 2017; **420**: 403–424. DOI 10.1016/j.desal.2017.06.025.

[10] Li Z., Linares R.V., Bucs S., Fortunato L., Hélix-nielsen C., Vrouwenvelder J.S., et al., *Desalination*, 2017; **420**: 208–215. DOI 10.1016/j.desal.2017.07.015.

[11] Blandin G., Verliefde A.R.D., Comas J., Rodriguez-Roda I., and Le-Clech P., *Membranes*, 2016; **6(3)**: 37–61. DOI 10.3390/membranes6030037.

[12] Amin P.D., Bhanushali V., and Joshi S., *Int. J. ChemTech. Res.*, 2018; **11(9)**: 247–259. DOI 10.20902/ijctr.2018.110932.

[13] Milescu R.A., McElroy C.R., Farmer T.J., Williams P.M., Walters M.J., and Clark J.H., *Adv. Polym. Tech.*, 2019; **2019**: 1–15. DOI 10.1155/2019/9692859.

[14] Peydayesh M., Bagheri M., Mohammadi T. and Bakhtiari O., *RSC Adv.*, 2017; **7(40)**: 24995–25008. DOI 10.1039/c7ra03566g.

[15] Qin H., Nie S., Cheng C., Ran F., He C., Ma L., et al., *Polym. Adv. Technol.*, 2014; **25(8)**: 851–860. DOI 10.1002/pat.3316.

[16] Nasr M., Alfryyan N., Ali S.S., Abd El-Salam H.M. and Shaban M., *RSC Adv.*, 2022; **12(39)**: 25654–25668. DOI 10.1039/d2ra03832c.

[17] Alvi M.A.U.R., Khalid M.W., Ahmad N.M., Niazi M.B.K., Anwar M.N., Batool M., et al., *Adv. Polym. Tech.*, 2019; **2019**: 8074626. DOI 10.1155/2019/8074626.

[18] Pellegrin B., Prulho R., Rivaton A., Thérias S., Gardette J., Gaudichet-Maurin E., et al., *J. Membrane Sci.*, 2013; **447**: 287–296. DOI 10.1016/j.memsci.2013.07.026.

[19] Syafiq M.A.W., and Rahman S.A., *Chiang Mai J. Sci.*, 2018; **45(1)**: 484–491.

[20] Arthanareeswaran G. and Starov V.M., *Desalination*, 2011; **267(1)**: 57–63. DOI 10.1016/j.desal.2010.09.006.

[21] Abdullah M.A.M., Abu Seman M.N., Tuan Chik S.M S., and Abdullah S.B., *Process Saf. Environ.*, 2022; **161**: 34–49. DOI 10.1016/j.psep.2022.03.016.

[22] Akther N., Sodiq A., Giwa A., Daer S., Arafat H.A., and Hasan S.W., *Chem. Eng. J.*, 2015; **281**: 502–522. DOI 10.1016/j.cej.2015.05.080.

[23] Cai Y., Shen W. Wei J., Chong T.H., Wang R., bKrantz W.B., et al., *Environ. Sci.-Wat. Res.*, 2015; **1(3)**: 341–347. DOI 10.1039/C4EW00073K.

[24] Zhong Y., Feng X., Chen W., Wang X., Huang K., Gnanou Y., et al., *Environ. Sci. Technol.*, 2016; **50(2)**: 1039–1045. DOI 10.1021/acs.est.5b03747.

[25] Phang S.N., Syed M.S., Abdullah S.B., Abu Seman M.N., and Mohd Taib M., *Malaysian J. Anal. Sci.*, 2018; **22(4)**: 605–611.

[26] Zeweldi H.G., Bendoy A.P., Park M.J., Shon H.K., Johnson E.M., Kim H., et al., *Chemosphere*, 2021; **263**: 128070. DOI 10.1016/j.chemosphere.2020.128070.

[27] Haddad A.Z., Menon A.K., Kang H., Urban J., Prasher R.S., and Kostecki R., *Environ. Sci. Technol.*, 2021; **55**: 3260–3269. DOI 10.1021/acs.est.0c06232.

[28] Abdullah M.A.M., Man M.S., Phang S.N., Syed M.S., and Abdullah S.B., *J. Eng. Sci. Technol.*, 2019; **14(2)**: 1031–1042.

[29] Shafie N.A., Abu Seman M.N., Saufi S.M., and Mohammad A.W., *Chem. Eng. Res. Des.*, 2023; **200**: 186–201. DOI 10.1016/j.cherd.2023.10.034.

[30] Long Q., Qi G., and Wang Y., *ACS Sustain. Chem. Eng.*, 2016; **4(1)**: 85–93. DOI 10.1021/acssuschemeng.5b00784.

[31] Achilli A., Cath T.Y., and Childress A.E., *J. Membrane Sci.*, 2010; **364(1–2)**: 233–241. DOI 10.1016/j.memsci.2010.08.010.

[32] Phillip W.A., Yong J.U.I.S., and Elimelech M., *Environ. Sci. Technol.*, 2010; **44(13)**: 5170–5176.

[33] Güneş-Durak S., Ormancı-Acar T., and Tüfekci N., *Water Sci. Technol.*, 2017; 2017(2): 329–339. DOI 10.2166/wst.2018.142.

[34] Wang Y., Li X., and Wang R., *J. Membrane Sci.*, 2017; **541**: 73–84. DOI 10.1016/j.memsci.2017.06.088.

[35] Chun Y., Qing L., Sun G., Roil M., and Fane A.G., *Desalination*, 2018; **445**: 75–84. DOI 10.1016/j.desal.2018.07.030.

[36] Wang M., Wang Z., Wang X., Wang S., Ding W., and Gao C., *Environ. Sci. Technol.*, 2015; **49**: 3761–3768. DOI 10.1021/es5056337.

[37] Wei J., Qiu C., Tang C.Y., Wang R., and Fane A.G., *J. Membrane Sci.*, 2011; **372**: 292–302. DOI 10.1016/j.memsci.2011.02.013.

[38] Yang E., Chae K., and Kim I.S., *J. Chem. Technol. Biotechnol.*, 2015; **91**: 2305–2312. DOI 10.1002/jctb.4817.

[39] Phillip W.A., Schiffman J.D., and Elimelech M., *Environ. Sci. Technol.*, 2010; **44(10)**: 3812–3818.

[40] Wu H., Zhao H., Lin Y., Liu X., Yao H., Yu L., et al., *Sep. Purif. Technol.*, 2022; **297**: 121553. DOI 10.1016/j.seppur.2022.121553.

[41] Li Y., Xu Z., Xie M., Zhang B., Li G., and Luo W., *J. Membrane Sci.*, 2020; **593**: 117436. DOI 10.1016/j.memsci.2019.117436.

[42] Xia L., Andersen M.F., Nielsen C.H., and Mccutcheon J.R., *Ind. Eng. Chem. Res.*, 2017; **56(41)**: 11919–11925. DOI 10.1021/acs.iecr.7b02368.

[43] Abdullah M.A.M., Man M.S., Abdullah S.B., and Saufi S.M., *Desalin. Water Treat.*, 2020; **206**: 165–176. DOI 10.5004/dwt.2020.26317.

[44] Surhone L.M., Timpledon M.T., and Marseken S.F., *Van't Hoff Factor. Beau Bassin*, Betascript Publishing, 2010.

[45] Pramanik B.K., Shu L., Jegatheesan J., Shah K., Haque N., and Bhuiyan M.A., *Process Saf. Environ.*, 2019; **126**: 53–59. DOI 10.1016/j.psep.2019.04.004.

[46] Zaviska F. and Zou L., *Desalination*, 2014; **350**: 1–13. DOI 10.1016/j.desal.2014.07.005.

[47] Zhao S., Zou L., and Mulcahy D., *J. Membrane Sci.*, 2011; **382(1–2)**: 308–315. DOI 10.1016/j.memsci.2011.08.020.

[48] Sivertsen E., Holt T., and Thelin W.R., *Membranes*, 2018; **8**: 1–13. DOI 10.3390/membranes8030039.

[49] Giagnorio M., Ricceri F., and Tiraferri A., *Water Res.*, 2019; **153**: 134–143. DOI 10.1016/j.watres.2019.01.014.

[50] Zhang J., Wu J., Yu J., Zhang X., He J., and Zhang J., *Mater. Chem. Front.*, 2017; **1(7)**: 1273–1290. DOI 10.1039/C6QM00348F.

[51] Verma C., Mishra A., Chauhan S., Verma P., Srivastava V., Quraishi M.A., et al., *Sustain. Chem. Pharm.*, 2019; **13**: 100162. DOI 10.1016/j.scp.2019.100162.